AIAA JOURNAL
Vol. 37, No. 7, July 1999

Penetration and Mixing of Fully Modulated Turbulent Jets in Crossflow

H. Johari,* M. Pacheco-Tougas,† and J. C. Hermanson*
Worcester Polytechnic Institute, Worcester, Massachusetts 01609-2280

Fully modulated, incompressible, turbulent transverse jets were studied experimentally in a water tunnel over a range of pulsing frequencies and duty cycles and at two jet-to-crossflow velocity ratios. The jet flow was completely modulated by operating an in-line solenoid valve resulting in the shutoff of jet supply during a portion of the cycle. The planar laser-induced fluorescence technique was used to determine the penetration, dilution, and structural features of the pulsed jets. The molecular mixing rate was quantified using a chemical reaction between the jet and crossflow fluids. Short injection times resulted in creation of vortex ring structures, whereas long injection times produced axially elongated turbulent puffs, similar to a segment of a steady jet. The latter case resulted in only modest enhancement of the jet penetration depth and dilution. Pulsed jets dominated by vortex rings had penetration depths significantly greater than a steady jet with the same velocity ratio, up to a factor of 5 at 50 jet diameters downstream of the exit. For short injection times, duty cycle had a significant effect on the behavior of pulsed jets. Increasing the duty cycle for a fixed injection time reduced the jet penetration. The dilution and mixing of pulsed jets with short injection time was also improved over the steady jet for duty cycles as high as 0.5. The greatest increase in the mixing rate was approximately 50% for well-separated pulses with short injection times.

Introduction

TURBULENT transverse jets have many practically important applications, such as the combustion of a fuel jet in a crossflowing airstream, cooling of combustion chamber walls, discharge of chimney gases into the atmosphere, and thrust control. For this reason, and because of the improved mixing characteristics of these jets compared with freejets, e.g., Refs. 1 and 2, this flow configuration has been the subject of considerable study. Still, many important aspects of transverse jets, especially for the case of unsteady jet injection, are not fully understood.

Before considering how unsteady injection can modify the penetration and mixing of transverse jets, we will briefly summarize the known behavior of steady transverse jets. Three separate regions can be identified in the transverse jet, namely, the near field, including the potential core; the maximum deflection or transition region; and finally, the far field. These three regions are schematically shown in Fig. 1a. The potential core is characterized by a nearly uniform velocity and concentration. In the transition region, the jet deflects more substantially, and in the normal (y–z) plane, it deforms (in the mean) in a kidney-shaped fashion. Fearn and Weston,[3] using detailed velocity measurements, attributed the kidney-shaped profile to a pair of counter-rotating, streamwise vortices. This counter-rotating vortex pair appears to play an important role in the mixing of the jet.[1] Other types of structures associated with transverse jets are discussed by Fric and Roshko,[4] including jet shear-layer vortices, the horseshoe vortices, and wake vortices. Recent work by Smith and Mungal[5] confirmed the three regions of the jet already mentioned.

The current state of understanding of transverse turbulent jets is presented in the review article by Margason.[6] Most of the early research on transverse jets was more concerned with the jet trajectory and velocity profiles rather than with the structures associated with the jet or the jet mixing properties. The jet penetration and flow similarity was investigated by Keffer and Baines.[7]

The mean jet spreading rate was examined by Pratte and Baines,[8] who developed an expression for the trajectory of the jet centerline in terms of the velocity ratio (ratio of the jet exit velocity to crossflow velocity). The mean velocity distributions, the turbulence intensity, and mean temperature field of heated, transverse jets were surveyed by Kamotani and Greber,[2] who characterized the jet penetration in terms of the momentum ratio. Broadwell and Breidenthal[1] presented an analytical description of the jet far field, resulting in power-law scalings for the jet penetration and mixing with velocity ratio. Similar scaling laws for the jet trajectory and the decay of scalar concentration were obtained by Hasselbrink and Mungal[9] using a control-volume approach. Karagozian[10] examined analytically the dynamics of the streamwise vortices and their implications for jet penetration.

Unsteady injection has been seen to impact the growth and mixing characteristics of freejets without crossflow. Crow and Champagne[11] observed that small periodic forcing at the jet exit could produce a large increase in the near-field spreading rate. Favre Marinet and Binder[12] and Vermeulen et al.[13] studied the effects of high-amplitude acoustic pulsing of the jet and observed an increase in entrainment up to a certain downstream location from the jet exit. Bremhorst and Hollis,[14] in a study on fully-modulated freejets, found that the entrainment rate was approximately twice that of the steady jet with the same mean nozzle velocity. In a transverse jet, acoustic pulsation was studied by Vermeulen et al.[15] They found a significant increase in jet spread, and a penetration increase of up to 92% was observed, along with a corresponding decrease in jet mixing length. Kelso et al.[16] also forced a transverse jet, at a frequency close to that of the shear layer surrounding the jet, with an amplitude equal to 10% of the jet exit velocity. They observed an increase in the size of vortex rings found in the jet near field.

Fully modulating the jet, i.e., turning the jet completely off during part of each pulsation cycle, can drastically modify the flowfield and significantly increase penetration compared to the steady jet. Experiments with fully modulated liquid transverse jets in crossflow by Eroglu and Breidenthal[17] revealed up to 100% increase in jet penetration while the overall mixing rate (as indicated by the "flame" length) of the jet was increased by 50% at an optimum pulsing frequency. A study by Wu et al.[18] indicated that at low pulsing frequencies a jet injected into a crossflow can penetrate up to four times deeper than a steady jet for the same mean momentum flux.

Eroglu and Breidenthal[17] concluded that the vortex rings created because of pulsing are a determining factor in the increased penetration. The vortex rings penetrate deeply into the crossflow because

Presented as Paper 98-2908 at the AIAA 29th Fluid Dynamics Conference, Albuquerque, NM, 15–18 June 1998; received 31 August 1998; revision received 21 December 1998; accepted for publication 13 January 1999.

*Associate Professor, Mechanical Engineering Department. Senior Member AIAA.

†Graduate Student, Mechanical Engineering Department; currently Engineer, Pratt and Whitney, United Technologies Corporation, East Hartford, CT 06108.

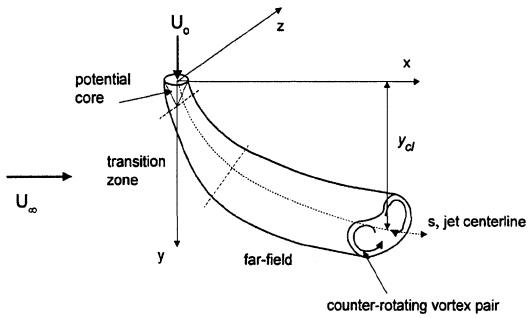

Fig. 1a Schematic of a transverse jet.

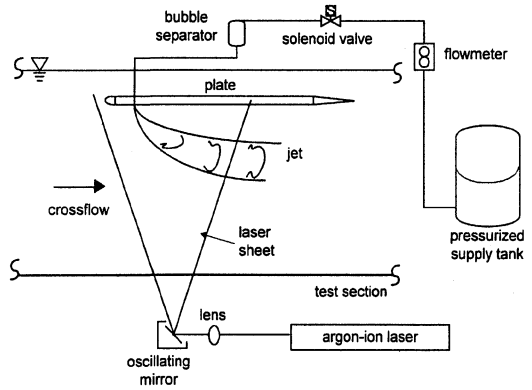

Fig. 1b Experimental apparatus.

of the self-induced velocity of the rings.[19] However, the distance between the sequential rings decreases as the frequency increases, resulting in increased interaction between the rings and reduced penetration.[17] By contrast, the use of a longer injection time can give rise to pulsed jets, which consist of a series of turbulent puffs, rather than compact vortex rings.[20]

In most of the past experiments with pulsed transverse jets, the percentage of jet-on during each cycle (the duty cycle α) was fixed at $\alpha = \frac{1}{2}$. Additionally, they all have generally been more concerned with the penetration of the jet and with the jet flowfield, rather than the mixing characteristics of the jet. An initial study of the effects of duty cycle on the structure of fully modulated transverse jets was conducted by Hermanson et al.[20] Controlling the duty cycle as an independent parameter allows the separate specification of the injection time and frequency, with implications for both the structure of jet puffs and the nature of their interaction. The injection time can be considered as a measure of the intensity of individual puffs, with shorter times leading to compact vortex rings and longer times to turbulent puff-like structures. The duty cycle (fraction of jet-on during each cycle) can be correspondingly viewed as a rough measure of the distance between the jet puffs.[20]

In this work we performed a systematic examination of the effects of duty cycle and injection time τ (related through the frequency $f = \alpha/\tau$) on the penetration and mixing of a transverse jet. The injection time and duty cycle were independently varied to reveal differences on the structure of the jet pulses and their interactions and the consequences for both penetration and mixing. The experiments were conducted on an incompressible turbulent transverse jet. The jet was fully modulated at low frequencies of 0.5–5 Hz and at three duty cycles of 0.5, 0.3, and 0.2. Planar laser-induced fluorescence (PLIF) of disodium fluorescein was utilized to visualize the flow and to measure the mean jet penetration and spreading rate and the concentration of a passive scalar. Chemically reactive jets were employed to quantify molecular scale mixing.

Experimental Setup

The experiments were performed in Worcester Polytechnic Institute's recirculating free-surface water tunnel. The clear Plexiglas® walls enclosing the 61 × 61 cm^2 test section allowed for flow visualization. The freestream velocity U_∞ was held at 15 cm/s in the present experiments, and various velocity ratios were obtained by changing the jet flow rate. The turbulence intensity in the test section was measured to be approximately 1%.

Jet Apparatus

The jet was mounted flush with the bottom surface of a flat plate submerged 13 cm below the free surface of the tunnel. The plate was 58 cm in width, 143 cm in length, and 1.3 cm in thickness. The gap between the plate and tunnel walls was filled with foam rubber. The leading edge of the plate had an elliptical section to avoid flow separation. The jet exit (0.3 cm diam) was located 4.4 cm downstream from the plate leading edge. The laminar boundary-layer thickness at this location was calculated to be less than 3 mm. The plate was positioned to remove any pressure gradient along the plate. A schematic of the setup is shown in Fig. 1b.

Jet fluid was supplied by a diaphragm tank charged with compressed air. The internal pressure was kept constant by adjusting a precision regulator. A rotameter at the exit of the supply tank allowed for the determination of the jet flow rate under steady operation. A small solenoid valve with a 2.9-mm orifice diameter was used for pulsing the jet flow. Downstream of the solenoid valve, a 3.1-cm-diam cylindrical reservoir removed any bubbles formed by the valve pulsation. A 10-cm-long stainless-steel tubing of 0.3-cm i.d. completed the piping immediately before the jet exit. A total of about 400 tube diameters between the cylindrical reservoir and the jet exit ensured a fully developed pipe flow profile under steady conditions. Two bulk jet velocities of 75 and 150 cm/s under steady conditions resulted in jet-to-crossflow velocity ratios of 5 and 10, respectively. The Reynolds numbers based on these velocities and the jet exit diameter were 2250 ± 50 and 4500 ± 100.

To ensure buoyancy effects were negligible in the experiments, the temperatures of the jet fluid was adjusted to match the freestream as closely as possible. It is estimated that, as a worst case, jet fluid was warmer than the freestream by 3°C. The length scale arguments of List[21] place transverse jets in the momentum-dominated region as long as the jet centerline penetration is less than the parameter $rd(\rho_o U_\infty^2/\Delta\rho g d)^{1/3}$. This condition was satisfied in all our runs, and thus, buoyancy did not have a significant effect on the jet flowfield.

The complete modulation of the jet flow was achieved by opening and closing of the solenoid valve, which had a response time of a few milliseconds. A square wave generated by a function generator was fed into a logic circuit with eight equally spaced settings to produce duty cycles between $\frac{1}{8}$ and 1. The amplified output of the circuit drove the solenoid valve. Nominal duty cycles α of $\frac{1}{2}$, $\frac{1}{4}$, and $\frac{1}{8}$ were employed with six pulsing frequencies f of 0.5, 1, 2, 3, 4, and 5 Hz, corresponding to jet Strouhal numbers (fd/U_0) ranging from 9×10^{-4} to 2.5×10^{-2}. These Strouhal numbers are significantly smaller than those typically used for forcing of freejets. The actual values of duty cycle were determined from hot-film velocity measurements at the jet exit.

The jet volume flow rate was measured by the flowmeter during steady operation. The average jet flow rate under pulsatile conditions was determined by collecting the fluid discharged from the jet exit over a 60-s period. Three trials were performed for each frequency and duty-cycle combination. Initial measurements revealed that there can be a significant decrease in the mean jet velocity with short injection times as compared to the steady case, primarily because of the response time of the hydraulic system. To compensate, reservoir pressure and valve settings were adjusted to obtain jet flow rates comparable to the steady counterparts.

To measure the temporal behavior of the jet exit velocity under various pulsing conditions, hot-film anemometry was employed using a single sensor positioned $0.5d$ from the jet exit. At least 10 complete pulses were utilized for averaging purposes. A sample velocity trace is shown in Fig. 2 for pulsing frequency of 4 Hz at a (nominal) duty cycle of $\frac{1}{2}$. Deviation of the pulses from the square wave varied among different cases, depending on the flow conditions. Pulses with larger duty cycles deviated the least from square waves. The weak secondary peak apparent after each pulse did not result in separate slugs of fluid at the jet exit as determined by flow visualization. A complete set of velocity traces for all of the pulsed cases can be found in Ref. 22.

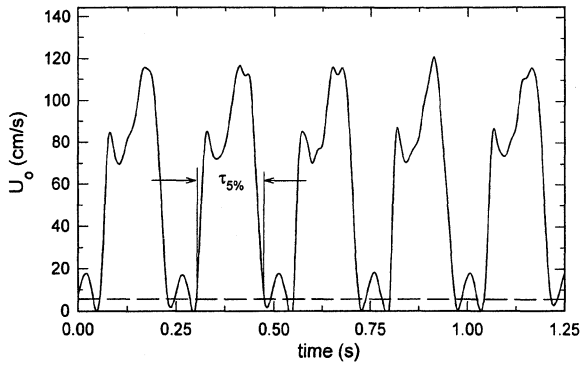

Fig. 2 Velocity trace of the pulsed jet at $r \approx 10$, $f = 4$ Hz, and nominal duty cycle of $\frac{1}{2}$; dashed line indicates a velocity equal to 5% of average peak velocity.

The actual injection time τ was defined based on 5% of the average peak velocity of the record (dashed line in Fig. 2). This injection time replaced the nominal value corresponding to the pulse length of the electronic square wave. Actual values of duty cycle were computed by multiplying the injection time by the pulsing frequency. The average duty cycles corresponding to the nominal values of $\frac{1}{2}$, $\frac{1}{4}$ and $\frac{1}{8}$ were 0.55 ± 0.01, 0.32 ± 0.02, and 0.21 ± 0.05 for the velocity ratio of 5 and 0.63 ± 0.04, 0.33 ± 0.03, and 0.23 ± 0.03 for the velocity ratio of 10.

To find the mean velocity U_0 of the pulsed jets during the injection interval, the measured volume flow rate was divided by the jet exit area and the calculated duty cycle for the specific pulsing condition. The jet Reynolds number and the corresponding velocity ratio ($r = U_0/U_\infty$) were computed using this average jet velocity. The values of Reynolds number were generally kept to within 20% of the steady jet values cited earlier. To estimate the standard error in the average jet exit velocity U_0, the error-propagation method was applied. The standard deviation of the mean jet exit velocity varied between 2 and 10% for the majority of the cases studied. The error increased with decreasing duty cycle.

Optical Setup

Flow visualization and passive scalar measurements were accomplished through the use of PLIF. The green line (514.5 nm) from an argon-ion laser, operated in the actively stabilized mode (0.5% rms noise level) was used to illuminate the flowfield. A planar light sheet was effectively formed by scanning the laser beam by a small mirror, where the period of the oscillation (frequency 1.2 kHz) was significantly shorter than the exposure time of the imaging system. A 1-m focal length lens was placed before the mirror to keep the beam collimated and to reduce the thickness of the laser sheet to $\approx$1 mm. The optical components were placed underneath the water tunnel test section, and the laser beam traveled upward, as shown in Fig. 1b. The laser beam was positioned to illuminate the jet symmetry plane.

The jet fluid consisted of a weak solution (5×10^{-6} M) of fluorescent dye (disodium fluorescein) in water. This concentration was chosen due to the linear response of the dye fluorescence intensity.[23] The low dye concentration also minimized the attenuation of the laser beam along its path, so that the fluorescence intensity at any point within the jet was linearly proportional to the local jet fluid concentration and the local laser beam intensity. Inasmuch as scanning the laser beam created nearly uniform illumination within the jet region of interest, the background-corrected fluorescence intensities revealed the local concentrations within the imaged plane. The uniformity of the laser illumination was verified by imaging the relevant area of the test section when it was filled with a uniform dye concentration of 1×10^{-7} M. The histogram of fluorescent intensities revealed that the illumination was very nearly uniform with a standard deviation of 3% of the mean value. The maximum attenuation of laser intensity was estimated to be 4.4%.

A progressive scan charge-coupled device (CCD) camera was used to capture images of the first 60 diameters of the fluorescing jet. The imager had a pixel resolution of 768×484 and a framing rate of 30 Hz. An orange filter effectively eliminated the scattered light from foreign particles. Camera images were acquired by means of a frame grabber installed in a personal computer. A total of 500 frames and at least 10 cycles of the pulsed jet were captured for each run. Mean concentration profiles of the transverse jet were extracted at axial stations from the jet exit to $50d$ at $5d$ spacing.

The spatial resolution of the data was determined by considering the 1 mm thickness of the laser sheet and the in-plane pixel resolution of 0.25×0.33 mm. The volumetric spatial resolution was, therefore, approximately 0.44 mm. This value is smaller than the viscous diffusion length scale,[24] calculated using the local jet width and velocity, and the proportionality constant suggested by Buch and Dahm,[24] beyond the $20d$ axial station. However, because the strain-limited scalar diffusion-layer thickness (Batchelor scale) is smaller than the viscous diffusion scale by the square root of the Schmidt number, the concentration measurements are underresolved by at least an order of magnitude. Thus, the concentration measurements reveal only the larger scale dilution and not the molecular-scale mixing rate. This was the primary reason for conducting experiments with chemically reactive jets described in the next section.

Fluorescent images of the jet were corrected by removing the background values found by averaging several images without the jet. This was done to exclude the fluorescence of the dye left in the tunnel from previous runs. The jet centerline penetration depth Y_{cl} at each axial station was defined as the point of maximum concentration of the profile. The ratio $C_{cl}(x)/C_0$ is commonly used to quantify the degree of jet dilution, where $C_{cl}(x)$ refers to the maximum of the average scalar concentration in the symmetry plane ($z = 0$) of the jet at location x and C_0 is the jet exit value. Transverse jets mix with crossflow fluid quite rapidly so that, at the farthest downstream measurement location of $50d$, the maximum jet fluid concentration was only about a few percent of the jet exit value for the steady case; pulsed jets diluted even faster in some cases. The CCD employed did not have enough dynamic range to resolve such large variations of the fluorescent intensity. To obtain sufficiently strong signals at $x = 50d$ for accurate measurements, the laser power was increased so that the jet images were saturated at the detector in the first few jet diameters. For this reason, the concentration at $x = 5d$ was chosen as the reference value and $C_{cl}(x)/C_{cl}(5d)$ as a measure of the degree of jet dilution at axial locations beyond $5d$. The concentration field for $x < 5d$ was not investigated.

The sources of error in the penetration and dilution rate measurements were due to (minute) laser sheet nonuniformity, optical alignment, A/D conversion, data extraction from digital images, and fluctuations of the turbulent flow. The accuracy of the measured mean jet penetration was $\approx 0.1d$. The uncertainty in fluorescence intensity of the images was estimated at 4%.

Chemically Reactive Jets

An isothermal chemical reaction between the jet fluid and the crossflow fluid was used to determine the molecular mixing rate of selected pulsed jets. This method has been used by Broadwell and Breidenthal[1] to measure the mixing rate of steady transverse jets. In the current experiments, the jet fluid consisted of an alkaline solution (NaOH) with a pH indicator (phenolphthalein), whereas the crossflow fluid contained nitric acid (HNO_3). The pH indicator is colorless in acidic solution and purple in alkaline solution with $pH \geq 9.8$. The mixing and chemical reaction between the colored jet and the crossflow neutralized the jet to the point that the jet became colorless due to the lack of OH^- ions. The mass of crossflow fluid needed to completely neutralize a unit mass of jet fluid (the equivalence ratio ϕ) can be adjusted by varying the relative strengths of the acid and the alkaline solutions. To accurately measure ϕ before each run, a titration was performed. The equivalence ratio was fixed in these runs at $\phi = 6.2$.

The location of the last jet fluid parcel to discolor, i.e., molecularly mix with the crossflow, reveals information about the minimum mixing rate of the jet. At this point all of the jet parcels are molecularly mixed to at least the prescribed equivalence ratio at the location of discoloration. The axial distance between this location and the jet exit will be denoted the reaction length L. The reaction length in the present experiments is analogous to the flame length of burning fuel jets, but without heat release effects. Because the reaction takes

place at the molecular level, a reduction in the reaction length for fixed ϕ indicates increased molecular mixing.

Chemically reacting jet images were recorded using the same camera used for the PLIF experiments. Spotlight illumination was used in these experiments, and the images were analyzed by an image processing program. Reaction lengths collected from 10 pulses for each condition were averaged. A gray-scale threshold level was established to guide the identification of the point at which the pH indicator discolored completely. In this manner, the measurement procedure was reasonably consistent for all of the runs.

Steady Jets

To verify that the apparatus created steady transverse jets consistent with previous studies, penetration, half-width, and dilution rate of steady jets with velocity ratios of 5 and 10 were measured. Additionally, these measurements established a benchmark against which pulsed jet measurements can be compared.

Instantaneous and time-averaged images of the steady jet with $r = 5$ are shown in Fig. 3. In all flow visualization images, the crossflow is from left to right with the jet issuing downward from the top left corner. The span of the images is $\approx 50d$ in the axial direction. The PLIF images are inverted so that darker regions indicate higher jet fluid concentration. The gray-scale map for the instantaneous images have been adjusted to varying degrees to reveal the flow structures more clearly, especially in the far field where the jet concentrations are very small.

The dilution and decrease of jet fluid concentration is clearly evident in the images of Fig. 3 especially in the transition region of the jet, $5d \leq x \leq 10d$ for this case. Also apparent is the presence of pure unmixed crossflow fluid parcels at several locations within the jet. The smooth concentration distribution shown in Fig. 3b over the entire region studied attests to the sufficient number of frames (500) used for averaging.

The jet centerline in the symmetry plane $z = 0$, Y_{cl}, was defined by the locus of maximum jet fluid concentration found from the averaged images. The penetration of the jet as indicated by Y_{cl} is presented in Fig. 4a, where the coordinates have been normalized by rd. The uncertainty of the normalized penetration is estimated to be 4.5%. Momentum flux arguments of Pratte and Baines[8] and Broadwell and Breidenthal[1] have shown that this scaling should remove the velocity ratio effects in the far field. The rd scaling results in a reasonable collapse of data. Possible sources of discrepancy between the two data sets are the different jet Reynolds numbers and the low signal levels at the farthest measurement location, especially in the $r = 10$ case.

As is customary, a power law of the form[1,8]

$$Y_{cl}/rd = A(x/rd)^n \tag{1}$$

was fitted to the data. The curve fit had a correlation coefficient greater than 95% and resulted in values of 1.7 and 0.25 for A and n, respectively. This power law is quite close to that obtained in the experimental studies of Pratte and Baines[8] and Niederhaus et al.[25] Past analytical work[1,9,10] has indicated a power of one-third for the far field of high velocity ratio transverse jets. A factor possibly affecting the difference between the experimental power law found here and that in analytical work is that the one-third power is deduced from vortex pair trajectory,[1,10] which may not necessarily coincide with the locus of maximum jet fluid concentration. In addition, the vortex cores are not located on the symmetry plane, and their trajectory has a different power law than the jet centerline.[3] The jet centerline based on the locus of the maximum velocity in the symmetry plane follows the one-third power law closely.[3] Both the best-fit curve and the one-third power law with proportionality constant 1.5 are also shown in Fig. 4a for comparison purposes.

The jet width δ, at one-half of peak concentration, was also extracted from the averaged images. The scaled jet width is plotted against the scaled penetration in Fig. 4b, where a linear dependence is expected. The uncertainty of the scaled jet width data is estimated at 5%. Past work[1,10] has shown that the jet width should scale the same way as the jet centerline. The data for both velocity ratios

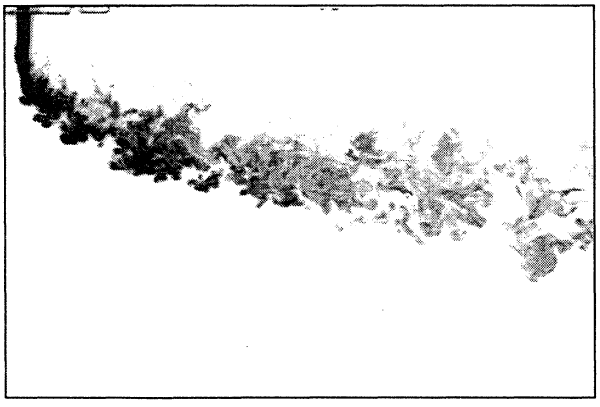

a) Instantaneous

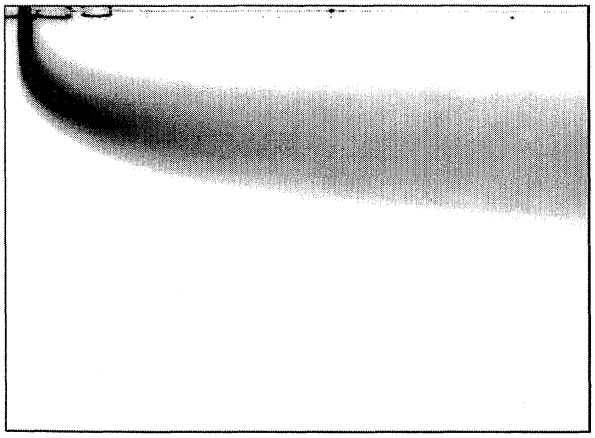

b) Averaged

Fig. 3 PLIF images of steady transverse jet with $r = 5$.

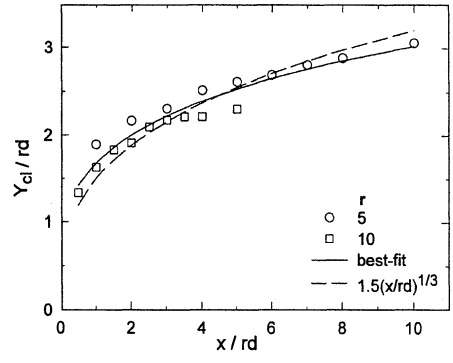

Fig. 4a Normalized penetration of steady transverse jets; solid and dashed curves represent the best-fit power law and the one-third scaling, respectively.

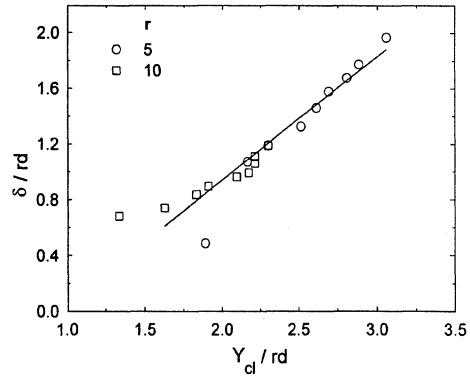

Fig. 4b Normalized width of the steady transverse jet as a function of normalized penetration; best-fit line to the data for $Y_{cl}/rd \geq 2$ has a slope of 0.9.

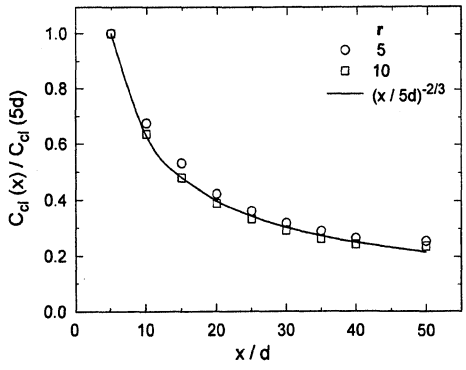

Fig. 5 Mean centerline concentration decay of steady transverse jets; solid curve indicates the far-field scaling of $(x/d)^{-2/3}$.

collapse quite well onto a single line with a slope of 0.9 for penetration depths beyond $2rd$. The transition region, in which the jet is aligning itself with the crossflow, is believed to cause the scatter at low penetration depths. Pratte and Baines[8] found that the vortex pair-dominated region starts at a penetration depth of approximately $2rd$, which corresponds to axial locations of approximately $10d$ and $19d$ for velocity ratios of 5 and 10, respectively, in our experiments. The penetration depth of $2rd$ is also consistent with the $0.2r^2d$ axial location suggested in Ref. 5 as the start of the far-field behavior.

The jet dilution can be quantified by the maximum concentration on the steady jet centerline divided by that at $x = 5d$, $C_{cl}(x)/C_{cl}(5d)$, as discussed earlier. The data are presented in Fig. 5, where the uncertainty is estimated at 4%. The experimental data nearly collapse for both velocity ratios and agree very well with the analytical expression $(x/5d)^{-2/3}$, derived from Broadwell and Breidenthal's[1] arguments for the far-field dilution rate. A similar expression for the dimensionless scalar concentration was developed by Hasselbrink and Mungal[9]:

$$\frac{C_{cl}}{C_0} = \left\{ 2\left(\frac{\rho_0}{\rho_\infty}\right) \Big/ \left[\frac{3}{A}\sqrt{\frac{\rho_\infty}{\rho_0}} r \left(\frac{x}{rd}\right)^{\frac{2}{3}} + 1 \right] \right\} \qquad (2)$$

Assuming uniform densities and neglecting unity in comparison with $r^{1/3}(x/d)^{2/3}$ in the denominator results in the same dependence on x/d as described earlier. The close correspondence between the two data sets and the analytical scaling is indicative of the validity of the measurement technique and the consistency of our steady jets with the past studies. When comparing the performance of pulsed jets with steady jets, $(x/5d)^{-2/3}$ will be used as the benchmark concentration decay rate. These results indicate that the behavior of the steady jets in the current work is consistent with that of previous studies.

Pulsed Jets

The flow structure, penetration, dilution, and reaction length of pulsed jets with various pulsing frequencies, injection times, and duty cycles are presented in this section. Because the two velocity ratios of 5 and 10 resulted in similar behavior, most data presented are from the $r = 5$ case. More extensive data for the $r = 10$ cases are available in Ref. 22.

Flow Visualization

The nature of flow structures in pulsed jets varied considerably with the pulsing parameters. The structures could essentially be classified into two categories. With long injection times, typically greater than ~300 ms, the injected jet pulse appeared similar to a portion of the steady jet in the far field, i.e., a turbulent flow segment elongated primarily in the direction of the crossflow. A sample of this type of structure is shown in Fig. 6, where only a single pulse is visible in the field of view. The jet of velocity ratio $r = 10$ was pulsed at 0.5 Hz with a duty cycle of $\alpha \approx 0.3$ resulting in an injection time of 650 ms. Note the similarity of the flow segment in Fig. 6 with the middle portion of Fig. 3a. Although a starting vortex ring almost always formed near the jet exit during the pulse initiation, the ring was quickly overtaken and broken up by the rest of the jet

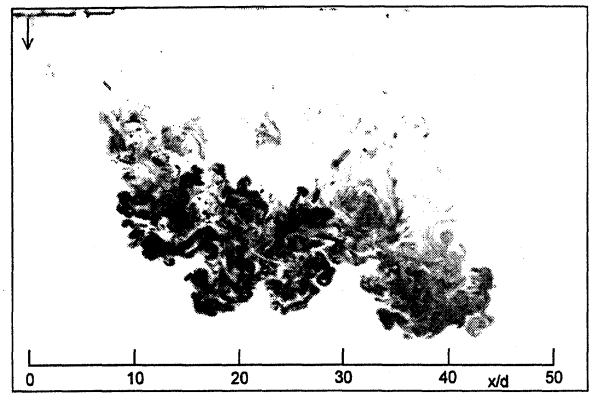

Fig. 6 Instantaneous image of a jet pulsed at 0.5 Hz with a duty cycle of 0.3; $\tau = 650$ ms and $r \approx 10$.

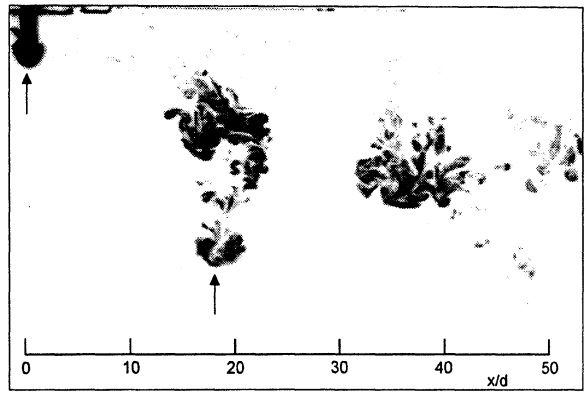

a) $f = 3$ Hz and $\tau = 110$ ms

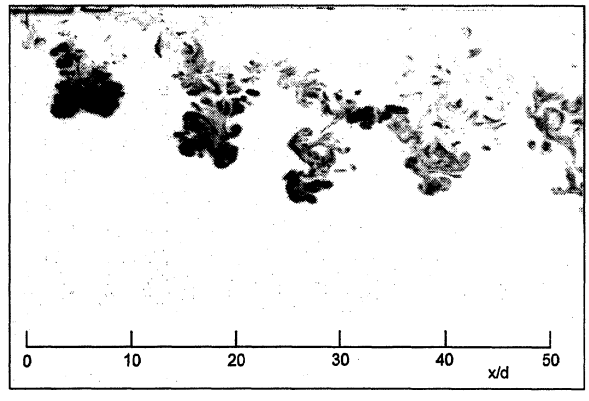

b) $f = 5$ Hz and $\tau = 70$ ms

Fig. 7 Instantaneous images of pulsed jets with $r \approx 5$ and duty cycle $\alpha \approx 0.3$.

fluid immediately behind it. Little evidence of organized vorticity could be found with this type of flow structure beyond the immediate vicinity of the jet exit.

With increased frequency and reduced injection time, the primary flow structures in the far field became more compact and stretched in the vertical direction, as opposed to the horizontally elongated structures for the long injection times. The images in Figs. 7a and 7b show pulsed jets at $r \approx 5$ and a duty cycle of $\alpha \approx 0.3$ and pulsing frequencies of 3 and 5 Hz (110- and 70-ms injection times). The presence of vertically oriented jet fluid parcels is evident in these images. The formation and persistence of compact fluid structures, which resemble vortex rings is also clearly evident in the 3-Hz case (Fig. 7a), where they are marked by arrows. The appearance of vortex rings in pulsed transverse jets has been reported by Eroglu and Breidenthal[17] and Wu et al.[18] at duty cycle of 0.5 and by Hermanson et al.[20] for $\alpha = 0.17$. It is believed that these vortex rings contribute to the greater penetration of the jet and rapid transport of momentum into the crossflow under pulsatile conditions.

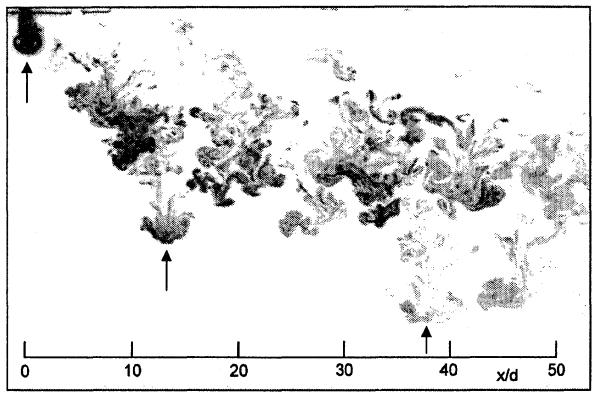

Fig. 8 Instantaneous image of a jet pulsed at $f = 5$ Hz with $\alpha \approx 0.5$ and $r \approx 5$.

The formation of a starting vortex is also depicted very clearly in Fig. 8, where the pulsing of the jet at 5 Hz and duty cycle 0.5 resulted in injection times of 100 ms. The vortex rings, again marked by arrows, are observed even in the far field in this case. Beyond the jet exit, the vortex rings became larger and asymmetric, with the upstream side of the core generally containing more concentrated jet fluid than the downstream side. The vortex rings of pulsed transverse jets are subject to the crossflow and possibly the wake of previous pulses and, therefore, would not be expected to remain as symmetrical as in the case of free vortex rings in quiescent surroundings. It is also important to point out that the injected pulses were not invariant for all values of pulsing parameters, as discussed earlier. Variations of the pulse shape may impact the formation and persistence of vortex rings among different pulsing cases.

A distinct feature of the flow in Figs. 7 and 8 is the separation between consecutive pulses. At a fixed duty cycle, increasing the frequency, which reduced the time interval between pulses, necessarily decreased the separation distance of successive pulses. For example, at a duty cycle of 0.3, no significant interaction, as indicated by the visual presence of pure ambient fluid, among neighboring pulses could be detected in the first $50d$ (see Fig. 7a). As the frequency increased from 3 to 5 Hz, the initial separation of consecutive pulses at the jet exit decreased. As a consequence of this reduction, the point at which successive pulses first interacted, i.e., visually observed entanglement of dyed fluid parcels from successive pulses or the disappearance of clear separating regions of fluid between pulses, moved closer to the jet exit. At 4 Hz, the pulses were interacting at approximately $40d$; at 5 Hz, the wake of consecutive pulses intermingled at approximately $35d$ (see Fig. 7b).

The reduction in the pulse separation was also observed when the frequency was fixed and the duty cycle increased, resulting in larger injection times. This also decreased the time interval between individual pulses near the nozzle. A comparison of the images in Figs. 7b and 8 reveals that at a fixed frequency of 5 Hz, the point of first interaction moved from roughly $35d$ at a duty cycle of 0.3 to approximately $27d$ at duty cycle of 0.5. Therefore, by decreasing the time between successive injections at the jet exit, the spatial separation among the pulses is reduced in the near field, leading to more rapid interaction among successive pulses. It is worth reiterating that the gray scale of the presented images does not linearly correspond to the actual concentrations, which are quite low in the far field.

Penetration

The mean penetration depth of pulsed jets, Y_{pulsed}, was defined at an axial location to be the y location of maximum scalar concentration of the averaged PLIF images for each pulsing condition. To make a meaningful comparison with steady jet penetration depths, pulsed jet measurements were normalized by the penetration of a steady jet with the same exit velocity as the mean velocity during each jet pulse. This normalization was done to compensate for the variation of the jet exit velocity with different pulsing parameters as discussed earlier. To calculate the penetration depth of a steady jet with an exit velocity equivalent to the pulsed jet, Eq. (1) was used

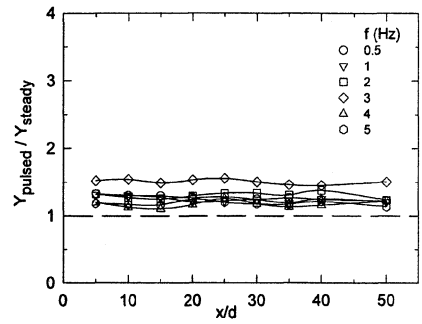

a) $\alpha \approx 0.5$

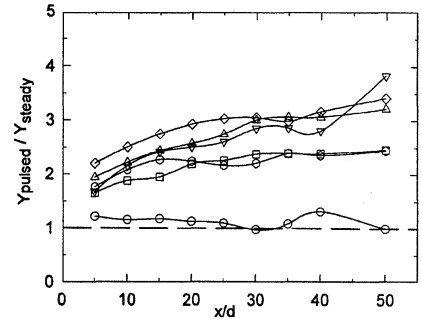

b) $\alpha \approx 0.3$

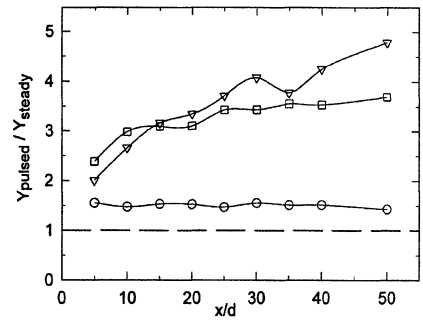

c) $\alpha \approx 0.2$

Fig. 9 Normalized penetration of $r \approx 5$ pulsed jets.

with A and n set at 1.7 and 0.25, respectively, and a velocity ratio corresponding to the actual value of pulsed jet.

The standard error of the normalized penetration ($Y_{\text{pulsed}}/Y_{\text{steady}}$) was affected by the uncertainty in the measurement of mean jet exit velocity during the jet-on time in additional to the uncertainty in Y_{pulsed} measurements. This error varied depending on the pulsing conditions, the uncertainty in pulsed jet exit velocity having the most significant weight in the expression. In general, the error ranged from 4 to 8%, whereas for the lowest duty cycles, it was close to 20%.

The normalized penetration as a function of axial location for various frequencies is presented in Figs. 9a–9c for the low velocity ratio ($r \approx 5$). The three graphs correspond to different duty cycles of $\alpha = 0.5$, 0.3, and 0.2. The graphs reveal that the penetration of pulsed jets is always greater than a steady jet with the same velocity ratio. The increase of penetration depth for pulsed jets with duty cycle $\alpha = 0.5$ was fairly modest and nearly independent of the axial distance from the jet exit. The largest increase of 50% over the steady case was associated with pulsing frequency of 3 Hz. The normalized penetration increased significantly for the two smaller duty cycles of 0.3 and 0.2. Except at the frequency of 0.5 Hz, the normalized penetration generally increased with the downstream distance for $\alpha \approx 0.3$ and 0.2, reaching as much as 380 and 480%, respectively, at $x = 50d$. Under these conditions, pulsed jets penetrated very rapidly in the near field; the rate of penetration increase diminished farther downstream. The highest normalized penetration was at frequencies of 3 and 1 Hz at these duty cycles. The results for the high-velocity ratio ($r \approx 10$) showed similar trends, with the

difference that significant penetration increase was also observed at the highest duty cycle of 0.5.

For the case where the penetration was comparable to that of the steady jet (0.5 Hz), the jets had the longest injection times at each duty cycle and the jet structure appeared as turbulent slugs stretched axially. With increased frequency, the injection time decreased, eventually transforming the structure of the jet from axially stretched turbulent puffs to more compact vortex ring structures. This structural change is accompanied by the observed increase in penetration. As injection time decreased further, the impulse of each pulse was reduced, ultimately weakening the vortex rings and leading to a decrease in normalized penetration. These effects also result in optimal frequencies for maximum penetration, depending on the duty cycle and velocity ratio. The penetration decreased once the frequency was increased beyond an optimum (see Fig. 9).

That the penetration of the pulsed jet decreases with increasing frequency, once a maximum has been reached, was also observed by Eroglu and Breidenthal.[17] In their study of pulsed jets with $\alpha = 0.5$, they observed that increasing the pulsing frequency beyond 5 Hz caused the penetration of the pulsed jet to decline toward that of the steady jet. Our data for low velocity ratio jets at duty cycle 0.5 agree qualitatively with those results.

Interpreting the observed penetration trends in terms of frequency is complicated because a change in frequency, for fixed duty cycle, alters the impulse of each pulse as well as the spatial and temporal spacing between successive pulses. To help isolate the duty cycle effect, penetration of pulsed jets with similar injection times, and therefore impulse, was examined. Penetration of pulsed jets with injection times of $\tau \approx 300$ and 200 ms is shown in Fig. 10. The uncertainty for the higher duty cycle data in these plots is 5%, whereas for the lower α it is about 10%. The significant effect of duty cycle on jet pulses with similar injection characteristics is clearly shown by the appreciable increases in penetration when duty cycle is reduced.

The spatial and temporal separation of consecutive pulses, as well as the structure of jet pulses, are determinant factors in the penetration of fully modulated jets. Well-separated vortex ring structures penetrated much deeper into crossflow. The duty cycle effects generally diminished when the structure of jet pulses changed to axially stretched puffs. Pulses with injection times of about 600 ms had very small penetration increases (~25%) over the steady jet and were not affected by the duty cycle, to within the experimental uncertainty.

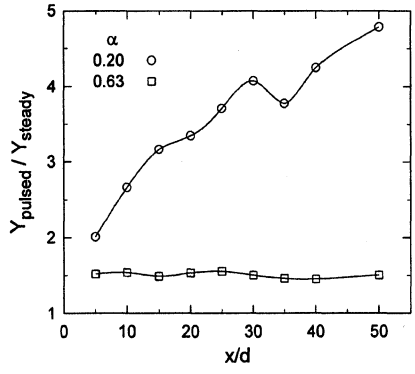

a) $\tau = 200$ ms

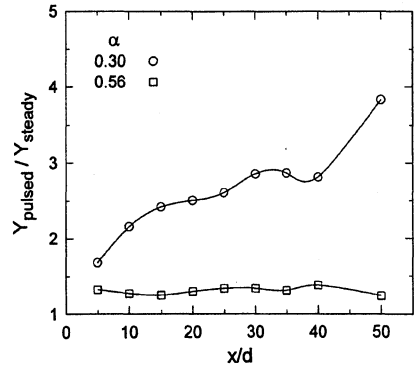

b) $\tau \approx 300$ ms

Fig. 10 Effect of duty cycle for $r \approx 5$ pulsed jets on normalized penetration at the indicated fixed injection times.

Dilution

Although jet pulses were synchronized with the primary pulsing frequency in the near field, the phase information was quickly lost and the pulses were effectively interacting with each other as early as $20d$ from the jet exit, depending on injection conditions. The loss of phase information was also observed in the near field of forced jets in Ref. 16. This presented a problem in using phase-averaged PLIF images to extract quantitative concentration values in the far field. The difficulty stems from the jet fluid concentration near the nozzle being effectively zero between successive pulses and the spatial and temporal spacing between neighboring pulses varying with downstream distance and pulsing conditions. To make an appropriate comparison of the concentration within individual jet pulses, the fluorescence intensity on the jet centerline was extracted from the recorded frames for each pulsing condition. The intensity values were then averaged to arrive at the mean concentration on the jet centerline, skipping the values corresponding to the pure crossflow fluid between successive pulses. At least 12 pulses were included in each average.

The jet dilution at any axial location was quantified by the ratio of the mean concentration on the pulsed jet centerline to that at a reference location. The reference location for pulsed jets was at $x = 10d$ from the exit because at $x = 5d$ several of the conditions resulted in saturated fluorescence intensity at the detector due to the high concentrations in the vortex ring cores.

The dilution ratio $C_{cl}(x)/C_{cl}(10d)$ was calculated for pulsing conditions, where individual pulses could clearly be identified in the far field. The standard deviation of the mean dilution ratio, which was in the range of 8–12%, increased with frequency and/or duty cycle in part due to the difficulty in identifying individual pulses. It is noteworthy that this definition of dilution ratio addresses only the decay of the mean centerline concentration of jet pulses.

The dilution ratio for various pulsing parameters is presented in Fig. 11. The steady jet behavior is depicted by the $-\frac{2}{3}$ power law as discussed earlier. The data indicate that pulsed jets generally dilute more rapidly than the steady jet in the far field. A jet pulsed at 0.5 Hz with a duty cycle of 0.5 diluted approximately as fast as the steady jet because this jet consisted of axially elongated pulses similar to segments of the steady jet. On the other hand, jet pulses diluted approximately twice as fast as the steady jet when the flow was pulsed at 2 Hz and $\alpha \approx 0.2$. This jet consisted of vertically stretched structures, which were well separated throughout the range studied. The other cases investigated diluted faster than the steady jet to varying degrees, as seen in Fig. 11, where the solid line indicates the behavior of the steady jets. Moreover, the dilution ratio was approximately a constant fraction of the steady jet value throughout the axial range for each set of pulsing parameters.

Reducing the duty cycle at a fixed frequency generally increased the dilution rate of the jet. This can be observed from comparing the data for jets pulsed at 3 Hz with duty cycles of 0.5 and 0.3 and for the 2-Hz jets at duty cycles of 0.3 and 0.2. The reduction in duty cycle at a fixed frequency also brought about a reduction in

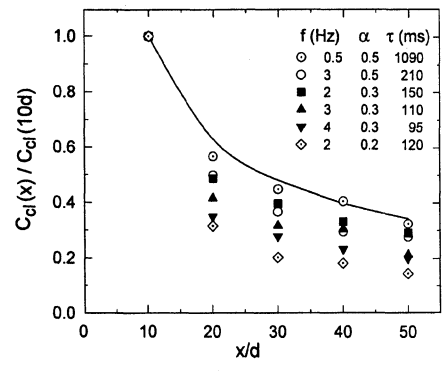

Fig. 11 Dilution ratio of $r \approx 5$ pulsed jets.

Table 1 Pulsing parameters of chemically reactive jets

r	f, Hz	α	τ, ms
5	3	0.5	210
	2	0.3	150
	3	0.3	110
	4	0.3	100
	2	0.2	120
10	4	0.5	170
	5	0.5	130
	3	0.3	120

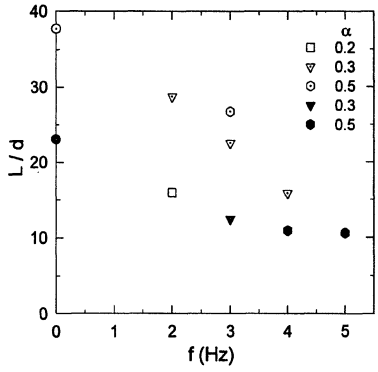

a) Reaction length L

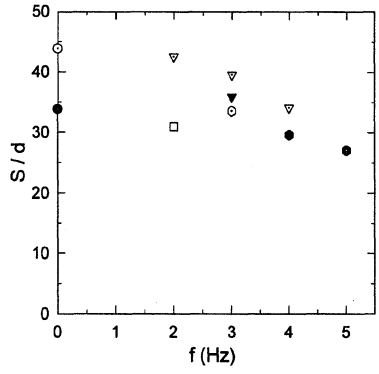

b) Reaction arclength S

Fig. 12 Chemically reactive jets at $\phi = 6.2$, open and filled symbols represent $r \approx 5$ and 10 cases, respectively; steady jet data at $f = 0$ Hz are shown as circles.

the injection time with an accompanying increase in the separation among consecutive pulses. Both of these effects are thought to be beneficial in enhancing the far-field dilution rate because pulses containing small amounts of jet fluid and being well separated from their neighbors would dilute rapidly. Holding the duty cycle constant while increasing the frequency also reduced the injection time and increased the temporal separation at the jet exit, again resulting in enhanced dilution in the far field. Data from jets with duty cycles of 0.3 and 0.5 in Fig. 11 show this trend. Thus, the reduction of the injection time is not the only parameter affecting the dilution; both the pulse separation and the flow structure play a role in determining the dilution rate.

Reaction Lengths

The integrated mixing rate at the molecular level was examined by measuring the reaction length of chemically reactive jets. Chemically reactive jets were investigated for certain pulsing parameters that generally resulted in largest penetration depths. These cases had injection times ranging from 100 to 210 ms and are listed in Table 1. The equivalence ratio ϕ was fixed at 6.2.

The average reaction length L is plotted as a function of frequency in Fig. 12a. The uncertainty in L was estimated to be 7%. To verify that the steady jets had reaction lengths consistent with the measurements of Broadwell and Breidenthal,[1] the current data were compared with their expression for the reaction length of steady transverse jets. The expression contains the equivalence ratio ϕ, velocity ratio r, and jet exit area A_0 as follows:

$$L = k\sqrt{(A_0/r)}(\phi + 1)^{\frac{3}{2}} \tag{3}$$

The proportionality constant k was estimated to be 4.4 from the data in Ref. 1. The reaction length of steady jets in the current experiments was $37.7d$ and $23.1d$ for the velocity ratios of 5 and 10, respectively. These values are within 10% of the values predicted by Eq. (3). Considering that the velocity ratio of 10 is near the upper limit for the validity of Eq. (3) and the estimated uncertainty of our measurements, the current data are in reasonable agreement with the steady jet reaction lengths in Ref. 1.

The data in Fig. 12a indicate that the reaction length of pulsed jets was shorter than the steady jet ($f = 0$) at the same velocity ratio for all cases examined, indicating faster molecular mixing. At the velocity ratio of $r = 5$, jets pulsed at 2 Hz with $\alpha \approx 0.2$ and at 4 Hz with $\alpha \approx 0.3$ showed the largest reduction of approximately 57% when compared with the steady case. At the higher velocity ratio, the reaction length reduction of about 50% was comparable for the three pulsing frequencies of 3, 4, and 5 Hz. The smallest reduction of approximately 29% was observed for the duty cycle of $\alpha = 0.5$ at $r \approx 5$.

These results are in agreement with those reported by Eroglu and Breidenthal[17] at an equivalence ratio of $\phi = 7$. They observed a reduction in reaction length of 63% for a jet of $r = 5$ pulsed at 4 Hz with duty cycle of 0.5. The reduction was comparable (64%) for a jet of $r = 10$ under the same pulsing conditions. Although those reductions are somewhat greater than the ones observed in the current experiments, they indicate similar trends.

The dilution results presented in the last section agree qualitatively with the reaction length measurements. Both diagnostic methods revealed that the jet pulsed at 2 Hz and duty cycle of 0.2 had the fastest dilution and mixing rate among all of the cases examined, 50% faster dilution and 57% reduction in reaction length compared to the steady jet. Additionally, the jets pulsed at 2 and 3 Hz with duty cycles of 0.3 and 0.5, respectively, showed the least reduction in reaction length and dilution ratio among the cases studied. The qualitative consistency among dilution ratios extracted from PLIF images and reaction length data suggests that the larger scales of motion responsible for entrainment of crossflow fluid into the jet structures are primarily accountable for the improved mass mixing.

Note that the starting rings were not visible in the chemically reactive jets. A possible explanation may be that even though the vortex rings were present in the flow, premature mixing of the first jet parcels in the tube may have discolored them prior to injection. The reaction length of all of the examined cases was shorter than the axial point at which interaction among neighboring pulses were observed. In particular, consecutive pulses of jets at 4 and 5 Hz did not interact before $20d$; the reaction length of these cases was less than $20d$.

The reaction axial length L is indicative of the minimum length in the axial direction required for mixing every jet fluid parcel with the crossflow at the prescribed equivalence ratio ϕ. Because pulsed jets had significantly greater penetration depths than the steady jets, a more appropriate comparison of mixing between the steady and pulsed jets would be to examine the reaction arclength S of reacting jets. The arclengths (see Fig. 1a) were calculated from the penetration measurements and are plotted in Fig. 12b. The uncertainty of S values was assessed to be 10%. The arclengths of reacting jets, like the reaction axial length L, are also smaller than those of steady jets, to within our measurement accuracy. However, the reductions in pulsed jet reaction arclengths are much less than those of the corresponding reaction axial lengths. The largest reduction of 30% in S was associated with $r \approx 5$ jets pulsed at 2 Hz with $\alpha \approx 0.2$. Moreover, the reaction arclengths appear to decrease with frequency at a fixed duty cycle. This can be attributed to the smaller volume injected during each pulse. Contrasting the reaction arclengths of transverse jets against that of a steady freejet ($\approx 60d$ for this ϕ) reveals that transverse jets have faster mixing rates, at least in the first $50d$.

Summary and Conclusions

Fully modulated, incompressible, turbulent jets injected into a uniform crossflow were studied experimentally at the jet-to-crossflow velocity ratios of 5 and 10. Complete modulation of the jet flow was accomplished by opening and closing of a solenoid valve such that the jet supply was cut off during a portion of the cycle. The pulsing frequencies extended from 0.5 to 5 Hz, corresponding to jet Strouhal numbers from 9×10^{-4} to 2.5×10^{-2}, at duty cycles of 0.5, 0.3, and 0.2. The injection times ranged from over 1 s to less than 0.1 s. The PLIF technique was used to visualize the symmetry plane of the jet and to determine the penetration depth, dilution ratio, and structural features of the pulsed jets. An estimate of the molecular mixing rate was found by measurements of the reaction length resulting from an isothermal chemical reaction between the jet and crossflow fluids. Measurements of the penetration, concentration, and reaction length in the steady case revealed that the steady jet flow in the current work was consistent with those of previous studies.

Complete modulation of the jet flow altered the jet structure, penetration depth, and dilution and mixing of the jet to varying degrees. Generally, long injection times created axially elongated turbulent puffs that resembled a segment of the steady jet. Pulsed jets composed of these flow structures resulted in only modest enhancement of the jet penetration depth and dilution rate. Spacing between neighboring puffs, which was affected by the duty cycle, altered the jet penetration and mixing characteristics minimally. The flow structure prevalent in pulsed jets with short injection times were vortex rings traveling transversely to the crossflow with a wake. These structures exhibited a jet penetration depth significantly greater than that of a steady jet with the same velocity ratio. A penetration increase of up to five times the steady jet value at $50d$ was observed with 200 ms long pulses at $r \approx 5$. Duty cycle had a significant effect on the performance of pulsed jets with short injection times. Increasing the duty cycle for a fixed injection time reduced the separation of successive pulses resulting in diminished penetration.

The dilution, as indicated by PLIF measurements, and mixing, as measured using the chemical-reaction technique, of pulsed jets with short injection time was also improved in comparison with steady jets of comparable velocity ratios. The most reduction in reaction length was on the order of 50% of the steady jet for well-separated pulses of short injection times. This reduction corresponds to a doubling of mixing rate. Generally, pulsed jets at high velocity ratio had characteristics similar to the low-velocity-ratio jets.

It is important to emphasize that both pulsing frequency and duty cycle determine the injection time and separation time between successive pulses. The latter parameters largely determine the flow structures, penetration, and mass mixing characteristics. Varying the pulse spacing with duty cycle for a fixed injection time can be an effective strategy for control of jet trajectory and mixing. Well-separated jet pulses depend on the initial impulse for penetration and very short injection time result in a reduction of the impulse. Thus, there would be optimal pulsing conditions that create strong, well-separated vortex rings for maximum penetration. In the present range of parameters, injection times of approximately 100 ms resulted in the most improvements in both penetration and mixing.

Acknowledgments

The help of K. J. Desabrais and F. J. Weber with the experiments is gratefully acknowledged.

References

[1]Broadwell, J. E., and Breidenthal, R. E., "Structure and Mixing of a Transverse Jet in Incompressible Flow," *Journal of Fluid Mechanics*, Vol. 148, Nov. 1984, pp. 405–412.

[2]Kamotani, Y., and Greber, I., "Experiments on a Turbulent Jet in a Cross Flow," *AIAA Journal*, Vol. 10, No. 11, 1972, pp. 1425–1429.

[3]Fearn, R., and Weston, R. P., "Vorticity Associated with a Jet in a Cross Flow," *AIAA Journal*, Vol. 12, No. 12, 1974, pp. 1666–1671.

[4]Fric, T. F., and Roshko, A., "Vortical Structure in the Wake of a Transverse Jet," *Journal of Fluid Mechanics*, Vol. 279, Nov. 1994, pp. 1–47.

[5]Smith, S. H., and Mungal M. G., "Mixing, Structure and Scaling of the Jet in Crossflow," *Journal of Fluid Mechanics*, Vol. 357, Feb. 1998, pp. 83–212.

[6]Margason, R. J., "Fifty Years of Jet in Cross Flow Research," *Computational and Experimental Assessment of Jets in Cross Flow*, CP-534, AGARD, 1993, pp. 1-1–1-41.

[7]Keffer, J. F., and Baines, W. D., "The Round Turbulent Jet in a Cross-Wind," *Journal of Fluid Mechanics*, Vol. 15, Pt. 4, 1963, pp. 481–496.

[8]Pratte, B. D., and Baines, W. D., "Profiles of the Round Turbulent Jet in a Cross Flow," *Journal of the Hydraulics Division, ASCE*, Vol. 92, Nov. 1967, pp. 53–64.

[9]Hasselbrink, E. F., and Mungal, M. G., "An Analysis of the Time-Averaged Properties of the Far Field of the Transverse jet," AIAA Paper 96-0201, Jan. 1996.

[10]Karagozian, A. R., "An Analytical Model for the Vorticity Associated with a Transverse Jet," *AIAA Journal*, Vol. 24, No. 3, 1986, pp. 429–436.

[11]Crow, S. C., and Champagne, F. H., "Orderly Structure in Jet Turbulence," *Journal of Fluid Mechanics*, Vol. 48, Pt. 3, 1971, pp. 547–591.

[12]Favre Marinet, M., and Binder, G., "Structure des Jets Pulsants," *Journal des Mecanique*, Vol. 18, No. 2, 1979, pp. 355–394.

[13]Vermeulen, P. J., Ramesh, V., and Yu, W. K., "Measurements of Entrainment by Acoustically Pulsed Axisymmetric Air Jets," *Journal of Engineering for Gas Turbines and Power*, Vol. 108, July 1986, pp. 479–484.

[14]Bremhorst, K., and Hollis P. G., "Velocity Field of an Axisymmetric Pulsed, Subsonic Air Jet," *AIAA Journal*, Vol. 28, No. 12, 1990, pp. 2043–2049.

[15]Vermeulen, P. J., Chin, C., and Yu, W. K., "Mixing of an Acoustically Pulsed Air Jet with a Confined Crossflow," *Journal of Propulsion*, Vol. 6, No. 6, 1990, pp. 777–783.

[16]Kelso, R. M., Lim, T. T., and Perry, A. E., "An Experimental Study of Round Jets in Cross-Flow," *Journal of Fluid Mechanics*, Vol. 306, Jan. 1996, pp. 111–144.

[17]Eroglu, A., and Breidenthal, R. E., "Effects of Periodic Disturbances on Structure and Flame Length of a Jet in a Cross Flow," AIAA Paper 91-0317, Jan. 1991.

[18]Wu, J. M., Vakili, A. D., and Yu, F. M., "Investigation of the Interacting Flow of Nonsymmetric Jets in Crossflow," *AIAA Journal*, Vol. 26, No. 8, 1988, pp. 940–947.

[19]Chang, Y. K., and Vakili, A. D., "Dynamics of Vortex Rings in Crossflow," *Physics of Fluids*, Vol. 7, No. 7, 1995, pp. 1583–1597.

[20]Hermanson, J. C., Wahba, A., and Johari, H., "Duty-Cycle Effects on Penetration of Fully Modulated, Turbulent Jets in a Crossflow," *AIAA Journal*, Vol. 36, No. 10, 1998, pp. 1935–1937.

[21]List, E. J., "Turbulent Jets and Plumes," *Annual Review of Fluid Mechanics*, Vol. 14, 1982, pp. 189–212.

[22]Pacheco-Tougas, M., "Penetration and Mixing of Fully-Modulated Turbulent Jets in Crossflow," M.S. Thesis, Mechanical Engineering Dept., Worcester Polytechnic Inst., Worcester, MA, April 1998.

[23]Koochesfahani, M. M., "Experiments on Turbulent Mixing and Chemical Reactions in a Liquid Mixing Layer," Ph.D. Dissertation, Aeronautics Dept., California Inst. of Technology, Pasadena, CA, Jan. 1984.

[24]Buch, K. A., and Dahm, W. J. A., "Experimental Study of the Fine-Scale Structure of Conserved Scalar Mixing in Turbulent Shear Flows," *Journal of Fluid Mechanics*, Vol. 317, June 1996, pp. 21–71.

[25]Niederhaus, C. E., Champagne, F. H., and Jacobs, J. W., "Scalar Transport in a Swirling Transverse Jet," *AIAA Journal*, Vol. 35, No. 11, 1997, pp. 1697–1704.

J. P. Gore
Associate Editor